Generation of Slot Index Tables for Time-Hopping Pseudolites with the Constructed Congruence Codes

Yi HU [1], Baoguo YU [2], Zhixin DENG [2], Wenjuan YU [1]

[1] Dept. of Mechanical & Electrical Engineering, Chuzhou University, Chuzhou, China
[2] State Key Lab. of Satellite Navigation System & Equipment Technology, Shijiazhuang, China

{hygps607, wenj_yu}@163.com, yubg@sina.cn, cetc54007@ta.an

Submitted August 26, 2022 / Accepted February 2, 2023 / Online first February 22, 2023

Abstract. *The time-hopping (TH) pulsed pseudolite (PL) can be used to enhance the performance of global navigation satellite systems (GNSS), and the slot index table (SIT) is an important part to form this PL signal. In this paper, a new method to generate SITs for multiple PLs is proposed. The general process of the proposed method is that first different time-hopping slot index (THSI) base matrices are generated based on the constructed congruence codes, and then by combining several different THSI base matrices to constitute a new matrix, the SIT for a PL is formed. Further by changing the combined matrices, different SITs for different PLs can be generated. During this process, two critical factors that affect the performance of the given method, i.e., the collision or hit property of the generated THSI base matrix and the correlation property of the formed SIT, are analyzed in detail. The simulations given at the end of this paper show that compared with many other similar schemes, the SITs given by the proposed method can obtain better correlation performance and detection performance in the receiver, and these results also imply that the proposed method offers a more effective way to design this kind of PL signal.*

Keywords

Global Navigation Satellite Systems (GNSS), time-hopping pseudolite, slot index table (SIT), congruence codes

1. Introduction

The pseudolite (PL) is a kind of ground-based transmitter which can be used to enhance the signal availability and integrity of global navigation satellite systems (GNSS), or directly form an independent local positioning system with four or more PLs to replace GNSS satellites in GNSS-denied environments, such as deep indoors, underground parking places, and so on [1–5]. During applying the PL to these environments, it may bring the serious "near-far" interference to weak GNSS satellite signal or other weak PL signal in receiving end. To solve this problem, many methods have been proposed and now it is thought that the time-hopping (TH) pulsed PL signal is one of the relatively better methods [2–4, 6].

The TH pulsed PL signal is often realized by gating the continuous local-generated GNSS-like signal with a chain of TH pulses, and the positions of these pulses are controlled by a basic TH pattern or slot index table (SIT) which consists of multiple permutation sequences of time-hopping slot indices (THSIs) [2, 3, 7]. To get better performance, the design of a SIT requires [4, 8, 9]: 1) the THSIs in a SIT should be pseudo-random so that the spectral shape of the original GNSS-like signal can be maintained as much as possible after gating; 2) the spreading factor of the PL signal in one SIT period should be same as or larger than that of the original GNSS-like signal in one data period; 3) each PL should be assigned with a different SIT so that the receiver can further use the SIT to distinguish different PLs besides the pseudo-random noise (PRN) codes of the underlying GNSS-like signal.

To meet above design requirements, currently two main SIT generation methods are proposed. One is the stream-based and the other is the blocked-based [4]. For the former, THSIs of a SIT are generated by the linear feedback shift register [10]. The drawback of this method is that the number of the generated THSIs in one permutation period is often power of two (including zero value). Meanwhile, it may cause the tracking problem due to the yield of some unbalanced long TH pulse intervals [2]. For the latter, THSIs of a SIT are generated by number theory and stored in memory prior to use [3], [8]. Compared with the former, the number of THSIs generated with the block-based method in one permutation period can be theoretically any predetermined value, and this will bring convenience to design different TH pulsed PL signal for different satellite navigation system. The drawback of this block-based method is that the performance of a generated SIT is not quite good when the size of the SIT is relatively short, and permutation sequences of THSIs used for a SIT often need optimal selection so that they have low hits. Currently, some typical block-based SIT generation schemes have been presented and used.

DOI: 10.13164/re.2023.0113

For examples, in [11] a predesigned SIT shared by multiple PLs is proposed, and in [3] different predesigned SITs for different PLs named LocataLites are also provided. Unfortunately, due to some reasons the design details of THSIs are not given in these SIT generation schemes.

In this paper, a new block-based SIT generation method is proposed. The general process of the proposed method is that first different THSI base matrices are generated based on the constructed congruence codes, and then by combining several different THSI base matrices and selecting certain rows from the combined matrix to constitute a new matrix, the SIT for a PL is formed. Meanwhile, by changing the combined matrices, different SITs for different PLs can be generated. The flow chart of generating one SIT of a PL is shown as Fig. 1. Wholly speaking, the benefits of our proposed method are:

- With the proposed method, different SITs for different PLs can be generated. Meanwhile, compared with many other similar schemes [2, 3, 9], the relatively better SIT correlation performance and detection performance of the proposed method can be obtained.
- Unlike many existing results [12–14], the SIT given by the proposed method is combined by several THSI base matrices so that the spreading factor required by the PL can be met.

The rest of the paper is organized as follows. Section 2 gives the signal model of TH pulsed PL. Section 3 presents the detailed generation methods of THSI base matrices and different SITs, followed by the correlation property analyses of the formed SIT given in Sec. 4. Section 5 gives the SIT detection method of the received PL signal. Section 6 presents the simulations to verify the performance of the formed SITs. Finally, the paper is concluded in Sec. 7.

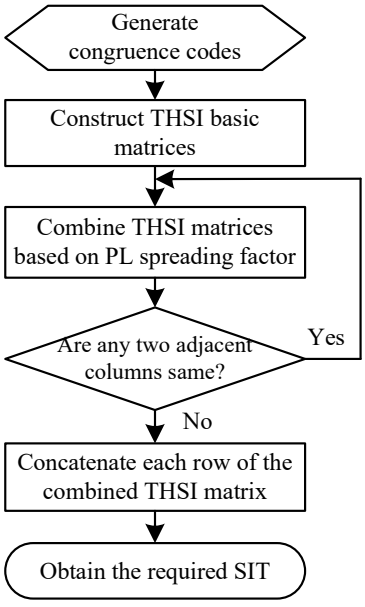

Fig. 1. Flow chart of generating one SIT of a TH pulsed PL.

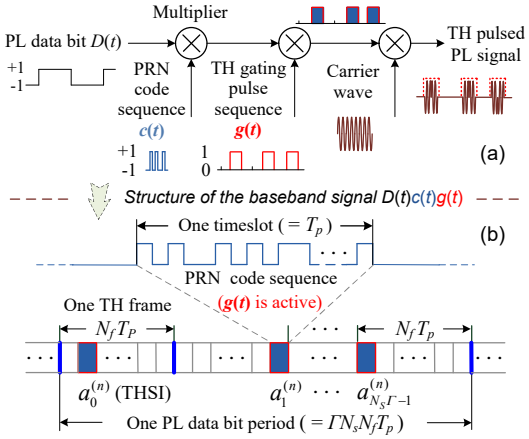

Fig. 2. Generation of the TH pulsed PL signal, in which (a) is the schematics and (b) is the structure of baseband signal.

2. TH Pulsed PL Signal Model

The generation of TH pulsed PL signal is shown in Fig. 2, in which the gating pulse $g(t)$ can be formulated as

$$g(t) = \sum_{n=-\infty}^{+\infty} \sum_{k=0}^{\Gamma N_s - 1} u_{T_p}\left(t - n\Gamma T_b - kT_c - a_k^{(n)} T_c d\right) \quad (1)$$

where T_b and T_c are periods of data bit and PRN code sequence of the original GNSS-like signal, respectively; d is the duty cycle of TH pulse which defines the duration of TH pulse $T_p \triangleq T_c d$ and the total slot number in one TH frame $N_f \triangleq 1/d$; the rectangle TH pulse $u_{T_p}(t) = 1$ in $0 \le t \le T_p$ and 0 otherwise; $N_s = T_b/T_c$ is the PRN code period repetitions in one GNSS-like signal data bit period, and Γ is the data bit period ratio of the PL signal to the original GNSS-like signal; $a_k^{(n)}$ is the THSI in the kth slot of the nth PL data bit and it randomly takes the value in the set $\{0, 1, \cdots, N_f - 1\}$, $\{a_k^{(n)}\}_{k=0}^{\Gamma N_s - 1}$ form the SIT of the PL signal [6]. Note that here Figure 2 is similar as Fig. 3 of reference [9] in SIT structure. Their main difference is that the former directly gives the SIT used in one data bit period, while the latter has divided the SIT used in one data bit period into multiple groups of random permutation sequences.

3. Generation of THSI Base Matrices and Different SITs

3.1 Construction of the Congruence Codes

From (1) it can be seen that the THSIs are critical to the generation of PL signal, in this paper motivated by the congruence codes given in [12] and [13], a series of new congruence codes used to generate THSIs is constructed by

$$x_{i,j}^{(l)} \equiv \left(\frac{(i+1)(j+1)}{l} - 1\right) (\mathrm{mod}\ p) \quad (2)$$

where p is a prime number; i, j, l are all integers and $0 \le i, j \le p-2$, $1 \le l \le p-1$. Then by the modular multiplicative inverse operation, it is easily derived that

$x_{i,j}^{(l)} \in \{0, 1, \cdots, p-2\}$ for $0 \le i, j \le p-2$ and $1 \le l \le p-1$. Meanwhile, for each pair of fixed parameters l and i, by changing j from 0 to $p-2$ the results of all $x_{i,j}^{(l)}$ can form a permutation which contains all elements of the set $\{0, 1, \cdots, p-2\}$ and has no common elements, and this is essential to generate the THSIs of the PL signal [2].

3.2 Generation of THSI Base Matrices

In (2), if take $j+1$, $i+1$ and l as the indices of TH frame, THSI permutation pattern related with the spreading factor of the PL signal [4] and THSI base matrix, respectively, meanwhile, let $N_\mathrm{f} = p-1$, then the constructed congruence codes can be used to generate different THSI base matrices to form different SITs. The structure of the generated THSI base matrix $\mathbf{X}^{(l)}$ is shown as Tab. 1, in which $x_{i,j}^{(l)} \in \{0, 1, \cdots, N_\mathrm{f}-1\}$ for $0 \le i, j \le N_\mathrm{f}-1$ and $1 \le l \le N_\mathrm{f}$.

For example, under $p = 5$ the four generated THSI base matrices with the proposed method are

$$\mathbf{X}^{(1)} = \begin{bmatrix} 0 & 1 & 2 & 3 \\ 1 & 3 & 0 & 2 \\ 2 & 0 & 3 & 1 \\ 3 & 2 & 1 & 0 \end{bmatrix}, \quad \mathbf{X}^{(2)} = \begin{bmatrix} 2 & 0 & 3 & 1 \\ 0 & 1 & 2 & 3 \\ 3 & 2 & 1 & 0 \\ 1 & 3 & 0 & 2 \end{bmatrix},$$

$$\mathbf{X}^{(3)} = \begin{bmatrix} 1 & 3 & 0 & 2 \\ 3 & 2 & 1 & 0 \\ 0 & 1 & 2 & 3 \\ 2 & 0 & 3 & 1 \end{bmatrix}, \quad \mathbf{X}^{(4)} = \begin{bmatrix} 3 & 2 & 1 & 0 \\ 2 & 0 & 3 & 1 \\ 1 & 3 & 0 & 2 \\ 0 & 1 & 2 & 3 \end{bmatrix}.$$

Note that here it has been assumed that $p = 1/d + 1$ to satisfy the given $N_\mathrm{f} = p-1$. When $p \ne 1/d+1$, the prime number which is larger than and nearest to $1/d+1$ can be used instead to generate the congruence codes. Thus in what follows only the case $p = 1/d + 1 = N_\mathrm{f} + 1$ is discussed.

Let $\mathbf{x}_{i_1}^{(l)} = \left[x_{i_1,0}^{(l)}, x_{i_1,1}^{(l)}, \cdots, x_{i_1,N_\mathrm{f}-1}^{(l)}\right]$ and $\mathbf{x}_{i_2}^{(l)} = \left[x_{i_2,0}^{(l)}, x_{i_2,1}^{(l)}, \cdots, x_{i_2,N_\mathrm{f}-1}^{(l)}\right]$ be two different rows taken from $\mathbf{X}^{(l)}$, where $i_1 \ne i_2$ and $1 \le l \le N_\mathrm{f}$. Meanwhile, define $\mathbf{x}_{i_2,\tau}^{(l)} \triangleq \left[x_{i_2,\tau}^{(l)}, x_{i_2,1\oplus\tau}^{(l)}, \cdots, x_{i_2,(N_\mathrm{f}-1)\oplus\tau}^{(l)}\right]$ and $\mathbf{X}_\tau^{(l)} \triangleq \left[x_{i,j\oplus\tau}^{(l)}\right]_{\substack{0\le i\le N_\mathrm{f}-1 \\ 0\le j\le N_\mathrm{f}-1}}$ the τ cyclic shift results of $\mathbf{x}_{i_2}^{(l)}$ and $\mathbf{X}^{(l)}$, respectively, where $\tau \in \mathbb{Z}$ and $0 < \tau \le N_\mathrm{f}-1$, "$\oplus$" denotes a modulo-$N_\mathrm{f}$ addition. Then the following results can be obtained.

$\mathbf{X}^{(l)} = \left[x_{i,j}^{(l)}\right]_{\substack{0\le i\le N_\mathrm{f}-1, \\ 0\le j\le N_\mathrm{f}-1}}$ $(1 \leqslant l \leqslant N_\mathrm{f})$		$j+1$ (index of TH frame)			
		1	2	$\cdots$	N_f
$i+1$ (index of THSI permutation pattern)	1	$x_{0,0}^{(l)}$	$x_{0,1}^{(l)}$	$\cdots$	$x_{0,N_\mathrm{f}-1}^{(l)}$
	2	$x_{1,0}^{(l)}$	$x_{1,1}^{(l)}$	$\cdots$	$x_{1,N_\mathrm{f}-1}^{(l)}$
	$\vdots$	$\vdots$	$\vdots$	$\ddots$	$\vdots$
	N_f	$x_{N_\mathrm{f}-1,0}^{(l)}$	$x_{N_\mathrm{f}-1,1}^{(l)}$	$\cdots$	$x_{N_\mathrm{f}-1,N_\mathrm{f}-1}^{(l)}$

Tab. 1. Structure of the generated THSI base matrix.

Theorem 1 The hit number of THSIs between $\mathbf{x}_{i_1}^{(l)}$ and $\mathbf{x}_{i_2,\tau}^{(l)}$ is at most one, where $\tau \in \mathbb{Z}$ and $0 < \tau \le N_\mathrm{f}-1$.

Proof: Suppose there are two hits between $\mathbf{x}_{i_1}^{(l)}$ and $\mathbf{x}_{i_2,\tau}^{(l)}$, then from (2) it can be derived that [15]

$$(i_1+1) \otimes (j_1+1) = (i_2+1) \otimes \left((j_1^{'}+1) \oplus \tau\right) \tag{3}$$

and

$$(i_1+1) \otimes (j_2+1) = (i_2+1) \otimes \left((j_2^{'}+1) \oplus \tau\right) \tag{4}$$

must hold simultaneously, where $j_1 \ne j_2$, $j_1^{'} \ne j_2^{'}$, and $j_1 - j_2 = j_1^{'} - j_2^{'}$, "$\otimes$" denotes a modulo-$N_\mathrm{f}$ multiplication.

By subtracting (3) with (4) it is easily derived that $i_1 = i_2$. This result will contradict the assumption $i_1 \ne i_2$, so there is at most one hit between $\mathbf{x}_{i_1}^{(l)}$ and $\mathbf{x}_{i_2,\tau}^{(l)}$. The same conclusion can be drawn for any two distinct columns of $\mathbf{X}^{(l)}$.

Theorem 2 The hit number of THSIs between $\mathbf{x}_{i_1}^{(l)}$ and $\mathbf{x}_{i_2,\tau}^{(l')}$ which come from $\mathbf{X}^{(l)}$ and $\mathbf{X}_\tau^{(l')}$, respectively, is at most N_f, where $0 \le i_1, i_2 \le N_\mathrm{f}-1$, $1 \le l, l' \le N_\mathrm{f}$, $l \ne l'$, $\tau \in \mathbb{Z}$ and $0 < \tau \le N_\mathrm{f}-1$, the definition of $\mathbf{x}_{i_2,\tau}^{(l')}$ is same as $\mathbf{x}_{i_2,\tau}^{(l)}$ except changing l to l'.

Proof: By subtracting (3) with (4) again after changing l to l' in the right terms of these two equations, it can be derived that $(i_1+1) \otimes (1/l) = (i_2+1) \otimes (1/l')$ will hold under $i_1 + 1 = l$ and $i_2 + 1 = l'$, and this implies that $\mathbf{x}_{i_1}^{(l)}$ may fully hit $\mathbf{x}_{i_2,\tau}^{(l')}$ or cause N_f hits. On the other hand, if $(i_1+1) \otimes (1/l) \ne (i_2+1) \otimes (1/l')$, then only one of equations (3) and (4) will hold, and this means the hit number between $\mathbf{x}_{i_1}^{(l)}$ and $\mathbf{x}_{i_2,\tau}^{(l')}$ is not more than one. Thus the THSI hit number between $\mathbf{x}_{i_1}^{(l)}$ and $\mathbf{x}_{i_2,\tau}^{(l')}$ is at most N_f under $l \ne l'$ and $\tau \in \mathbb{Z}$, $0 < \tau \le N_\mathrm{f}-1$.

3.3 Generation of Different SITs

Suppose one pulse is transmitted in one TH frame of the PL signal, then with the THSI base matrices given above, the SITs for different PLs can be formed. In fact, from Fig. 2 and Tab. 1 it is known that the number of THSIs required by a SIT is $\Gamma T_\mathrm{b}/T_\mathrm{c}$ and the number of THSIs in $\mathbf{X}^{(l)}$ is N_f^2, $1 \le l \le N_\mathrm{f}$. Thus by combining $N = \lceil \Gamma T_\mathrm{b}/(T_\mathrm{c} N_\mathrm{f}^2) \rceil$ different base matrices and randomly selecting $K = \Gamma T_\mathrm{b}/(T_\mathrm{c} N N_\mathrm{f})$ distinct rows from the combined matrix to constitute a new matrix $\mathbf{X}_K^{(l_1,l_2,\cdots,l_N)} = \left[\mathbf{X}_K^{(l_1)}\ \mathbf{X}_K^{(l_2)} \cdots \mathbf{X}_K^{(l_N)}\right]$, the SIT of a PL can be formed, where K should be equal or as close as possible to N_f so that the low hit performance of the formed SIT can be obtained, $l_1 \ne l_2 \cdots \ne l_N$ and $1 \le l_1, \cdots, l_N \le N_\mathrm{f}$, $\lceil \cdot \rceil$ denotes the ceil operation, $\mathbf{X}_K^{(l)}$ is a matrix formed by K selected rows of $\mathbf{X}^{(l)}$, $l = l_1, l_2, \cdots, l_N$. By repeating this process and changing part or whole values of l_1 to l_N, the SITs for different PLs can further be obtained.

$$\mathbf{X}_{10}^{(1,2)} = \Bigg[\underbrace{\begin{matrix} 0 & 1 & 2 & 3 & 4 & 5 & 6 & 7 & 8 & 9 \\ 1 & 3 & 5 & 7 & 9 & 0 & 2 & 4 & 6 & 8 \\ 2 & 5 & 8 & 0 & 3 & 6 & 9 & 1 & 4 & 7 \\ 3 & 7 & 0 & 4 & 8 & 1 & 5 & 9 & 2 & 6 \\ 4 & 9 & 3 & 8 & 2 & 7 & 1 & 6 & 0 & 5 \\ 5 & 0 & 6 & 1 & 7 & 2 & 8 & 3 & 9 & 4 \\ 6 & 2 & 9 & 5 & 1 & 8 & 4 & 0 & 7 & 3 \\ 7 & 4 & 1 & 9 & 6 & 3 & 0 & 8 & 5 & 2 \\ 8 & 6 & 4 & 2 & 0 & 9 & 7 & 5 & 3 & 1 \\ 9 & 8 & 7 & 6 & 5 & 4 & 3 & 2 & 1 & 0 \end{matrix}}_{\mathbf{X}_{10}^{(1)}} \quad \underbrace{\begin{matrix} 5 & 0 & 6 & 1 & 7 & 2 & 8 & 3 & 9 & 4 \\ 0 & 1 & 2 & 3 & 4 & 5 & 6 & 7 & 8 & 9 \\ 6 & 2 & 9 & 5 & 1 & 8 & 4 & 0 & 7 & 3 \\ 1 & 3 & 5 & 7 & 9 & 0 & 2 & 4 & 6 & 8 \\ 7 & 4 & 1 & 9 & 6 & 3 & 0 & 8 & 5 & 2 \\ 2 & 5 & 8 & 0 & 3 & 6 & 9 & 1 & 4 & 7 \\ 8 & 6 & 4 & 2 & 0 & 9 & 7 & 5 & 3 & 1 \\ 3 & 7 & 0 & 4 & 8 & 1 & 5 & 9 & 2 & 6 \\ 9 & 8 & 7 & 6 & 5 & 4 & 3 & 2 & 1 & 0 \\ 4 & 9 & 3 & 8 & 2 & 7 & 1 & 6 & 0 & 5 \end{matrix}}_{\mathbf{X}_{10}^{(2)}} \Bigg] \tag{5}$$

For example, suppose $T_b = 20\,\text{ms}$, $T_c = 1\,\text{ms}$, $\Gamma = 10$ and $d = 0.1$, just as what are used in Locata scheme [3], [6], then it can be derived that $\Gamma T_b/T_c = 200$, $N_f = 10$, $N = 2$ and $K = 10$, which means different SITs can be formed by $\mathbf{X}_{10}^{(l_1,l_2)} = \left[\mathbf{X}_{10}^{(l_1)}\ \mathbf{X}_{10}^{(l_2)}\right]$ under different values of l_1 and/or l_2, $l_1 \neq l_2$ and $1 \leq l_1, l_2 \leq 10$. For example, the generated SIT of $\mathbf{X}_{10}^{(1,2)}$ which is formed by $\mathbf{X}_{10}^{(1)}$ and $\mathbf{X}_{10}^{(2)}$ can be given as (5).

Generally speaking, the SITs formed by $\mathbf{X}_K^{(l_1,l_2)} = \left[\mathbf{X}_K^{(l_1)}\ \mathbf{X}_K^{(l_2)}\right]$ under different values of l_1 and/or l_2 are often enough for normal PL applications, where $l_1 \neq l_2$ and $1 \leq l_1, l_2 \leq N_f$. Note that in $\mathbf{X}_K^{(l_1,l_2)}$ the matrix $\mathbf{X}_K^{(l)} = \left[\mathbf{x}_0^{(l)}\,\mathbf{x}_1^{(l)} \cdots \mathbf{x}_k^{(l)} \cdots \mathbf{x}_{N_f-1}^{(l)}\right]$, where $\mathbf{x}_k^{(l)} = \left[x_{i_0,k}^{(l)}, x_{i_1,k}^{(l)}, \cdots, x_{i_{K-1},k}^{(l)}\right]^T$ in which $l = l_1, l_2$; $k = 0, 1, \cdots, N_f - 1$; i_0 to i_{K-1} are indices of K selected rows in $\mathbf{X}^{(l)}$, $0 \leq i_0 < \cdots < i_{K-1} \leq N_f - 1$, and $\mathbf{x}_{N_f-1}^{(l_1)} \neq \mathbf{x}_0^{(l_2)}$ so that the formed SIT has low hits. For simplicity, hereafter only the SIT formed by this $\mathbf{X}_K^{(l_1,l_2)}$ is discussed.

4. Correlation Property Analysis of the Formed SIT

4.1 Binary Mapping of the Formed SIT

From Fig. 1 it can be seen that the generation of the PL signal need map the formed SIT to binary code sequence. Meanwhile, the correlation property of the formed SIT, which is often used as a more intuitive way to characterize the hit property of the formed SIT, is also evaluated by the mapped binary code sequence. To fulfill this work of mapping, first K rows of $\mathbf{X}_K^{(l_1,l_2)}$ are concatenated sequentially to form an array $\mathbf{a}_{\text{SIT}}^{(l_1,l_2)} = \left[a_0^{(l_1,l_2)}, a_1^{(l_1,l_2)}, \cdots, a_k^{(l_1,l_2)}, \cdots, a_{2KN_f-1}^{(l_1,l_2)}\right]$, and then $\mathbf{a}_{\text{SIT}}^{(l_1,l_2)}$ is mapped into binary code sequence $\left\{\vartheta_i^{(l_1,l_2)}\right\}_{i=0}^{2KN_f^2-1}$ by

$$\vartheta_i^{(l_1,l_2)} = \begin{cases} 1, & i = a_k^{(l_1,l_2)} + kN_f,\ k \in \mathbb{Z}, 0 \leq k \leq 2KN_f - 1; \\ 0, & \text{otherwise.} \end{cases} \tag{6}$$

Note that here $\mathbf{a}_{\text{SIT}}^{(l_1,l_2)}$ is just $\left\{a_k^{(n)}\right\}_{k=0}^{\Gamma N_s-1}$ of (1), in which $\Gamma = K$ and $N_s = 2N_f$. Meanwhile, the above formed SIT, which has the size of $2KN_f$ and is subject to the spreading factor requirement of the PL signal, may not be optimal under some cases [14]. At this time the performance bound of the SIT can be obtained by the following Theorem 3 and Corollary 1. Additionally, from (6) the storage complexity of the binary-mapped SIT can be easily calculated to be $2KN_f^2$.

4.2 Auto- and Cross-Correlation Properties of the Formed SIT

With the obtained sequence $\left\{\vartheta_i^{(l_1,l_2)}\right\}_{i=0}^{2KN_f^2-1}$, the correlation property of the formed SIT can be evaluated by the auto-correlation function (ACF) and cross-correlation function (CCF) of $\left\{\vartheta_i^{(l_1,l_2)}\right\}_{i=0}^{2KN_f^2-1}$ which are defined as [15]

$$R_{\vartheta^{(l_1,l_2)}}(\tau) = \sum_{i=0}^{2KN_f^2-1} \vartheta_i{}^{(l_1,l_2)} \vartheta_{(i+\tau)\,(\text{mod } 2KN_f^2)}^{(l_1,l_2)} \tag{7}$$

and

$$C_{\vartheta^{(l_1,l_2)}}(\tau) = \sum_{i=0}^{2KN_f^2-1} \sum_{\substack{j=0, \\ j\neq i}}^{2KN_f^2-1} \vartheta_i^{(l_1,l_2)} \vartheta_{(j+\tau)\,(\text{mod } 2KN_f^2)}^{(l_1,l_2)}, \tag{8}$$

respectively, where τ is the cyclic shift of the mapped code sequence, $\tau \in \mathbb{Z}$ and $0 \leq \tau \leq 2KN_f^2 - 1$. For convenience, here the right shift of τ is chosen for analysis. Then based on (7) and (8) and Theorems 1 and 2, the properties of $R_{\vartheta^{(l_1,l_2)}}(\tau)$ and $C_{\vartheta^{(l_1,l_2)}}(\tau)$ can be given as follows.

Theorem 3 The subpeak upper bound of $R_{\vartheta^{(l_1,l_2)}}(\tau)$ normalized to $R_{\vartheta^{(l_1,l_2)}}(0)$ equals $(N_f + K - 1)/(KN_f)$, where $\tau \in \mathbb{Z}$ and $0 < \tau \leq 2KN_f^2 - 1$.

Proof: From (7) it is easily got that the subpeak upper bound of $R_{\vartheta^{(l_1,l_2)}}(\tau)$ equals the maximum hit number between $\left\{\vartheta_i^{(l_1,l_2)}\right\}_{i=0}^{2KN_f^2-1}$ and its τ cyclic shift result. Define $\xi_r \triangleq \lfloor \tau/(2N_f^2) \rfloor$, $\xi_h \triangleq \lfloor \tau/N_f^2 \rfloor$, $\xi_f \triangleq \lfloor \tau/N_f \rfloor$, $\tau_f \triangleq \xi_f N_f$ and $\tau_e \triangleq \tau (\text{mod } N_f)$, where $\lfloor \cdot \rfloor$ denotes the floor operation. Meanwhile, let $x_{i_\gamma,j}^{(l_1,l_2)}$ and $x_{u,v}^{(l_1,l_2)}$ be the elements

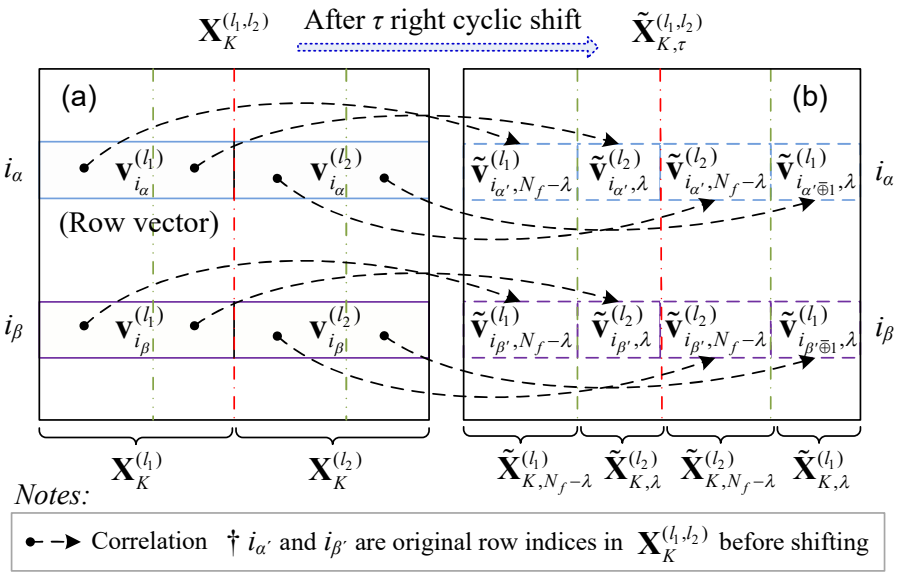

Fig. 3. Correlation between $\mathbf{X}_K^{(l_1,l_2)}$ and its τ cyclic shift result $\tilde{\mathbf{X}}_{K,\tau}^{(l_1,l_2)}$ under $\tau = \tau_\mathrm{f} + \tau_\mathrm{e}$, where $\tau_\mathrm{f} \neq 0$ and $\tau_\mathrm{e} \neq 0$.

of $\mathbf{X}_K^{(l_1,l_2)}$ and its equivalent τ cyclic shift result $\mathbf{X}_{K,\tau}^{(l_1,l_2)}$, respectively, where $\gamma, i_\gamma, j, u, v$ are all integers and they meet $0 \le \gamma \le K-1$, $0 \le i_\gamma, u \le N_\mathrm{f}-1$ and $0 \le j, v \le 2N_\mathrm{f}-1$. Then the previous maximum hit number also equals the maximum hit result between $\mathbf{X}_K^{(l_1,l_2)}$ and $\mathbf{X}_{K,\tau}^{(l_1,l_2)}$ when τ takes a certain value and the following relationships are satisfied: $u = i_{\gamma \bar{\oplus} \xi_\mathrm{r}}$, $v = (j + \xi_\mathrm{f}) (\mathrm{mod}\ 2N_\mathrm{f})$ and $x_{u,v}^{(l_1,l_2)} = x_{i_\gamma,j}^{(l_1,l_2)} \oplus \tau_\mathrm{e}$, where "$\bar{\oplus}$" denotes a modulo-$K$ addition. Based on this idea, the hits between $\mathbf{X}_K^{(l_1,l_2)}$ and $\mathbf{X}_{K,\tau}^{(l_1,l_2)}$ under different τ and above relationships can be first given as follows.

1) When $\tau = 2\eta N_\mathrm{f}^2$ where $\eta \in \mathbb{N}$ and $1 \le \eta \le K-1$, the parameters $\tau_\mathrm{f} = \tau$ and $\tau_\mathrm{e} = 0$. At this time $\mathbf{X}_{K,\tau}^{(l_1,l_2)}$ can be written as $\mathbf{X}_{K,\tau}^{(l_1,l_2)} = \left[\mathbf{X}_{K,\xi_\mathrm{r}}^{(l_1)}\ \mathbf{X}_{K,\xi_\mathrm{r}}^{(l_2)}\right]$, where $\mathbf{X}_{K,\xi_\mathrm{r}}^{(l)} = \left[\mathbf{x}_{\xi_\mathrm{r},0}^{(l)}\ \mathbf{x}_{\xi_\mathrm{r},1}^{(l)}\ \cdots\ \mathbf{x}_{\xi_\mathrm{r},m}^{(l)}\ \cdots\ \mathbf{x}_{\xi_\mathrm{r},(N_\mathrm{f}-1)}^{(l)}\right]$ in which $\mathbf{x}_{\xi_\mathrm{r},m}^{(l)} = \left[x_{i_{\xi_\mathrm{r}},m}^{(l)}, x_{i_{\xi_\mathrm{r}\bar{\oplus}1},m}^{(l)}, \cdots, x_{i_{\xi_\mathrm{r}\bar{\oplus}(K-1)},m}^{(l)}\right]^\mathrm{T}$, $m = 0, 1, \cdots, N_\mathrm{f}-1$; $l = l_1, l_2$. Then from Theorem 1 it is easily derived that the total hits between $\mathbf{X}_K^{(l_1,l_2)}$ and $\mathbf{X}_{K,\tau}^{(l_1,l_2)}$ are at most $2K$ because they in fact consist of the self hits between: $\mathbf{X}_K^{(l_1)}$ and $\mathbf{X}_{K,\xi_\mathrm{r}}^{(l_1)}$, $\mathbf{X}_K^{(l_2)}$ and $\mathbf{X}_{K,\xi_\mathrm{r}}^{(l_2)}$, both of which equal K at most.

2) When $\tau = (2\eta-1)N_\mathrm{f}^2$ where $\eta \in \mathbb{N}$ and $1 \le \eta \le K$, the parameters $\tau_\mathrm{f} = \tau$ and $\tau_\mathrm{e} = 0$. At this time $\mathbf{X}_{K,\tau}^{(l_1,l_2)}$ can be written as $\mathbf{X}_{K,\tau}^{(l_2,l_1)} = \left[\mathbf{X}_{K,\xi_\mathrm{r}}^{(l_2)}\ \mathbf{X}_{K,\xi_\mathrm{r}}^{(l_1)}\right]$, where the definition of $\mathbf{X}_{K,\xi_\mathrm{r}}^{(l)}$ is same as that given in 1), $l = l_1, l_2$. Then from Theorem 2 it is easily derived that the total hits between $\mathbf{X}_K^{(l_1,l_2)}$ and $\mathbf{X}_{K,\tau}^{(l_1,l_2)}$ are at most $2(N_\mathrm{f}+K-1)$ because they consist of the cross hits between: $\mathbf{X}_K^{(l_1)}$ and $\mathbf{X}_{K,\xi_\mathrm{r}}^{(l_2)}$, $\mathbf{X}_K^{(l_2)}$ and $\mathbf{X}_{K,\xi_\mathrm{r}}^{(l_1)}$, both of which equal $N_\mathrm{f}+K-1$ at most. Note that here only one pair of rows between $\mathbf{X}_K^{(l_1)}$ and $\mathbf{X}_{K,\xi_\mathrm{r}}^{(l_2)}$, or between $\mathbf{X}_K^{(l_2)}$ and $\mathbf{X}_{K,\xi_\mathrm{r}}^{(l_1)}$, may cause N_f hits at most under the given cyclic shift τ.

3) When τ takes other values except those given in 1) and 2), i.e., the parameters $\tau_\mathrm{f} \neq 0$ and $\tau_\mathrm{e} \neq 0$ for this case. At this time $\mathbf{X}_{K,\tau}^{(l_1,l_2)}$ can be written as $\tilde{\mathbf{X}}_{K,\tau}^{(l_1,l_2)} = \left[\tilde{\mathbf{X}}_{K,N_\mathrm{f}-\lambda}^{(l_1)}\ \tilde{\mathbf{X}}_{K,\lambda}^{(l_2)}\ \tilde{\mathbf{X}}_{K,N_\mathrm{f}-\lambda}^{(l_2)}\ \tilde{\mathbf{X}}_{K,\lambda}^{(l_1)}\right]$ when ξ_h takes an odd number, or $\tilde{\mathbf{X}}_{K,\tau}^{(l_2,l_1)} = \left[\tilde{\mathbf{X}}_{K,N_\mathrm{f}-\lambda}^{(l_2)}\ \tilde{\mathbf{X}}_{K,\lambda}^{(l_1)}\ \tilde{\mathbf{X}}_{K,N_\mathrm{f}-\lambda}^{(l_1)}\ \tilde{\mathbf{X}}_{K,\lambda}^{(l_2)}\right]$ when ξ_h takes an even number, where $\lambda = (\tau - \xi_\mathrm{h} N_\mathrm{f}^2)/N_\mathrm{f}$ denotes the TH frame shift number and $0 < \lambda < N_\mathrm{f}$. Here the relationship between $\mathbf{X}_K^{(l_1,l_2)}$ and $\tilde{\mathbf{X}}_{K,\tau}^{(l_1,l_2)}$ is shown as Fig. 3, in which the matrices $\tilde{\mathbf{X}}_{K,\lambda}^{(l)} = \left[\tilde{\mathbf{x}}_{\xi_\mathrm{r},\tau_\mathrm{e},0}^{(l)}\ \tilde{\mathbf{x}}_{\xi_\mathrm{r},\tau_\mathrm{e},1}^{(l)}\ \cdots\ \tilde{\mathbf{x}}_{\xi_\mathrm{r},\tau_\mathrm{e},\lambda-1}^{(l)}\right]$ and $\tilde{\mathbf{X}}_{K,N_\mathrm{f}-\lambda}^{(l)} = \left[\tilde{\mathbf{x}}_{\xi_\mathrm{r},\tau_\mathrm{e},\lambda}^{(l)}\ \tilde{\mathbf{x}}_{\xi_\mathrm{r},\tau_\mathrm{e},\lambda+1}^{(l)}\ \cdots\ \tilde{\mathbf{x}}_{\xi_\mathrm{r},\tau_\mathrm{e},N_\mathrm{f}-1}^{(l)}\right]$, where $\tilde{\mathbf{x}}_{\xi_\mathrm{r},\tau_\mathrm{e},m}^{(l)} = \left[x_{i_{\xi_\mathrm{r}},m}^{(l)} \oplus \tau_\mathrm{e}, x_{i_{\xi_\mathrm{r}\bar{\oplus}1},m}^{(l)} \oplus \tau_\mathrm{e}, \cdots, x_{i_{\xi_\mathrm{r}\bar{\oplus}(K-1)},m}^{(l)} \oplus \tau_\mathrm{e}\right]^\mathrm{T}$, $m = 0, 1, \cdots, N_\mathrm{f}-1$. Because the maximum hit number between $\mathbf{X}_K^{(l_1,l_2)}$ and $\tilde{\mathbf{X}}_{K,\tau}^{(l_2,l_1)}$ is same as that between $\mathbf{X}_K^{(l_1,l_2)}$ and $\tilde{\mathbf{X}}_{K,\tau}^{(l_1,l_2)}$, here only the latter case is considered. Then from Fig. 3 it is easily seen that the hits between $\mathbf{X}_K^{(l_1,l_2)}$ and $\tilde{\mathbf{X}}_{K,\tau}^{(l_1,l_2)}$ in fact consist of: a) the partial self hits between $\mathbf{X}_K^{(l_1)}$ and $\tilde{\mathbf{X}}_{K,N_\mathrm{f}-\lambda}^{(l_1)}$; b) the partial cross hits between $\mathbf{X}_K^{(l_1)}$ and $\tilde{\mathbf{X}}_{K,\lambda}^{(l_2)}$; c) the partial self hits between $\mathbf{X}_K^{(l_2)}$ and $\tilde{\mathbf{X}}_{K,N_\mathrm{f}-\lambda}^{(l_2)}$; and d) the partial cross hits between $\mathbf{X}_K^{(l_2)}$ and $\tilde{\mathbf{X}}_{K,\lambda}^{(l_1)}$.

To get the partial self hits of case a), the first $N_\mathrm{f}-\lambda$ columns of $\mathbf{X}_K^{(l_1)}$ are chosen to correlate with $\tilde{\mathbf{X}}_{K,N_\mathrm{f}-\lambda}^{(l_1)}$. Because they come from the same THSI base matrix, based on Theorem 1 it can be got that the total partial self hit number between $\mathbf{X}_K^{(l_1)}$ and $\tilde{\mathbf{X}}_{K,N_\mathrm{f}-\lambda}^{(l_1)}$ is $N_\mathrm{f}-\lambda$ at most. This result is also true for the partial self hits of case c).

To get the partial cross hits of case b), two different rows of $\mathbf{X}_K^{(l_1,l_2)}$ denoted by $\mathbf{v}_{i_\alpha}^{(l_1,l_2)} = \left[\mathbf{v}_{i_\alpha}^{(l_1)}\ \mathbf{v}_{i_\alpha}^{(l_2)}\right]$ and $\mathbf{v}_{i_\beta}^{(l_1,l_2)} = \left[\mathbf{v}_{i_\beta}^{(l_1)}\ \mathbf{v}_{i_\beta}^{(l_2)}\right]$, as shown in Fig. 3(a), and two different shifted results of $\tilde{\mathbf{X}}_{K,\tau}^{(l_1,l_2)}$ denoted by

$\tilde{\mathbf{v}}_{i_{\alpha'},\lambda}^{(l_1,l_2)} = \left[\tilde{\mathbf{v}}_{i_{\alpha'},N_\mathrm{f}-\lambda}^{(l_1)}\ \tilde{\mathbf{v}}_{i_{\alpha'},\lambda}^{(l_2)}\ \tilde{\mathbf{v}}_{i_{\alpha'},N_\mathrm{f}-\lambda}^{(l_2)}\ \tilde{\mathbf{v}}_{i_{\alpha'\bar{\oplus}1},\lambda}^{(l_1)}\right]$ and $\tilde{\mathbf{v}}_{i_{\beta'},\lambda}^{(l_1,l_2)} = \left[\tilde{\mathbf{v}}_{i_{\beta'},N_\mathrm{f}-\lambda}^{(l_1)}\ \tilde{\mathbf{v}}_{i_{\beta'},\lambda}^{(l_2)}\ \tilde{\mathbf{v}}_{i_{\beta'},N_\mathrm{f}-\lambda}^{(l_2)}\ \tilde{\mathbf{v}}_{i_{\beta'\bar{\oplus}1},\lambda}^{(l_1)}\right]$, as shown in Fig. 3(b), are chosen to assist the analysis, where α, β, α' and β' are all taken from the set $\{0, 1, \cdots, K-1\}$ and here $\alpha' \neq \beta'$, $\alpha = \alpha' \bar{\oplus} \xi_\mathrm{r}$ and $\beta = \beta' \bar{\oplus} \xi_\mathrm{r}$. Then from Theorem 2 it can be got that when $\mathbf{v}_{i_\alpha}^{(l_1)}$ of $\mathbf{v}_{i_\alpha}^{(l_1,l_2)}$ and $\tilde{\mathbf{v}}_{i_{\alpha'}}^{(l_2)}$ of $\tilde{\mathbf{v}}_{i_{\alpha'},\lambda}^{(l_1,l_2)}$ in the i_αth row meet the condition $i_\alpha \otimes l_2 = i_{\alpha'} \otimes l_1$, they may cause λ hits; whereas for the other rows of $\mathbf{X}_K^{(l_1)}$ and $\tilde{\mathbf{X}}_{K,\lambda}^{(l_2)}$, they may cause $K-1$ hits at most totally. Thus the total cross hit number between $\mathbf{X}_K^{(l_1)}$ and $\tilde{\mathbf{X}}_{K,\lambda}^{(l_2)}$ is $\lambda + K - 1$ at most. This result is also true for the partial cross hits of case d) when the condition $i_\beta \otimes l_1 = (i_{\beta'\bar{\oplus}1}) \otimes l_2$ is met.

With the results of a) to d), the total hits between $\mathbf{X}_K^{(l_1,l_2)}$ and $\tilde{\mathbf{X}}_{K,\tau}^{(l_1,l_2)}$ under the case 3) can be given as $2(N_\mathrm{f} + K - 1)$ at most. Finally based on the results given in 1) to 3) and $R_{\vartheta^{(l_1,l_2)}}(0) = 2KN_\mathrm{f}$, the subpeak upper bound of $R_{\vartheta^{(l_1,l_2)}}(\tau)$ normalized to $R_{\vartheta^{(l_1,l_2)}}(0)$ can be easily calculated to be $(N_\mathrm{f} + K - 1)/(KN_\mathrm{f})$, where $\tau \in \mathbb{Z}$ and $0 < \tau \leq 2KN_\mathrm{f}^2 - 1$.

Similarly, the property of $C_{\vartheta^{(l_1,l_2)}}(\tau)$ can also be given as follows.

Corollary 1 The peak upper bound of $C_{\vartheta^{(l_1,l_2)}}(\tau)$ normalized to $R_{\vartheta^{(l_1,l_2)}}(0)$ equals $(N_\mathrm{f} + 2K - 2)/(KN_\mathrm{f})$, where $\tau \in \mathbb{Z}$ and $0 < \tau \leq 2KN_\mathrm{f}^2 - 1$.

5. SIT Detection of the Received PL Signal

Besides the generation of SITs for different PLs in transmitting end, the SIT detection of the PL signal in receiving end is also an important task for fulfilling the assistance function of the PL. Generally speaking, at this time the detection of the SIT is directly changed to search the TH pulse positions of the received PL signal, and this can be fulfilled by three steps: generating the auto-correlation peaks of PRN codes, calculating the pulse intervals of every two adjacent pulses, and using the obtained pulse intervals to find the pulse positions of the PL signal. In our previous work [9], this question has been investigated in detail. As a supplement to current work, the main process of the TH pulse detection will be roughly presented in following parts.

5.1 Generation of the Underlying PRN Code Auto-correlation Peaks

The purpose of generating the underlying PRN code auto-correlation peaks is to obtain the intervals of any two adjacent TH pulses within one TH pulse pattern. Before this, it first requires to acquire the PRN code initial phase so that the auto-correlation peaks can be correctly generated. On the other hand, though the received pulsed PL signal is discontinuous at this time, the method of acquiring the PRN code initial phase of continuous GNSS satellite signal still can be applied to the PL signal [7].

Based on Fig. 2 and using the parallel PRN code phase search acquisition method [16], the principle of acquiring the PRN code initial phase τ_prn of the received PL signal can be given as

$$\tau_\mathrm{prn} = \arg\left(\max_{\hat{\tau}_c} \sqrt{I_{\hat{c}_m}^2(\hat{\tau}_\mathrm{c}, \hat{f}_\mathrm{Dop}) + Q_{\hat{c}_m}^2(\hat{\tau}_\mathrm{c}, \hat{f}_\mathrm{Dop})}\right) \quad (9)$$

where $\hat{\tau}_\mathrm{c}$, $\hat{f}_\mathrm{Dop}$, and $\{\hat{c}_m\}_{m=0}^{M-1}$ are the estimated PRN code initial phase, Doppler frequency, and PRN code sequence of the PL signal, respectively; $I_{\hat{c}_m}(\hat{\tau}_\mathrm{c}, \hat{f}_\mathrm{Dop})$ and $Q_{\hat{c}_m}(\hat{\tau}_\mathrm{c}, \hat{f}_\mathrm{Dop})$ are in-phase and quadrature phase integration results of two consecutive TH frames, respectively, and their detailed forms can be referred to [9].

With (9), the local generated baseband signal can be written as $s_{\hat{c}_m}(\tau_\mathrm{prn}) = \sum_{m=0}^{M-1} \hat{c}_m u_{T_\mathrm{ch}}\left(t - mT_\mathrm{ch} - \tau_\mathrm{prn}\right)$, where T_ch is the period of one PRN code chip. Then by correlating $s_{\hat{c}_m}(\tau_\mathrm{prn})$ with the received PL signal in each interval $\left[\gamma N_\mathrm{f} T_\mathrm{p}, (\gamma+1)N_\mathrm{f} T_\mathrm{p}\right]$, the auto-correlation peaks of underlying PRN code sequence and their positions can be easily found, where $\gamma = 0, 1, \cdots, \lfloor \Delta t/(N_\mathrm{f} T_\mathrm{p}) \rfloor - 1$ and Δt is the signal collection time.

5.2 Calculation of the TH Pulse Intervals

To improve the detection probability, the binary code sequence mapped from the auto-correlation peak intervals are often used to detect the SIT of the PL signal. Suppose N_t auto-correlation peaks have been found and their positions are $\{p_k, k = 0, 1, \cdots, N_\mathrm{t} - 1\}$, then TH pulse intervals of the PL signal in unit of T_p can be calculated by

$$\Lambda_{k-1,k} = \left\lfloor \frac{p_k - p_{k-1}}{T_\mathrm{p} f_\mathrm{s}} \right\rfloor, \quad k = 1, 2, \ldots, N_\mathrm{t} - 1 \quad (10)$$

where f_s is the sampling frequency.

Based on (10), the TH pulse interval set can be given as $\left\{\Lambda_{k-1,k}, k = 1, 2, \cdots, N_\mathrm{t} - 1\right\}$. From this the mapped binary code sequence can be obtained by $\mathbf{H} = \left\{h(i), i = 0, 1, \cdots, \sum_{k=1}^{N_\mathrm{t}-1}\right\}$, where the element

$$h(i) = \begin{cases} 1, & i = \sum_{k=1}^{J} \Lambda_{k-1,k},\ J = 0, 1, 2, \cdots, N_\mathrm{t} - 1; \\ 0, & \text{others.} \end{cases} \quad (11)$$

Similar as the derivation of the binary code sequence mapped from the auto-correlation peak intervals, each SIT table stored in the receiver can also be mapped into binary code sequence. More concretely, the binary code sequence mapped from the ζ-th SIT of total N stored results can be given as $\mathbf{B}^{(\zeta)} = \left\{b^{(\zeta)}(i), i = 0, 1, \cdots, 2KN_\mathrm{f} - 1\right\}$, where $\zeta = 1, 2, \cdots, N$, and the element

$$b^{(\zeta)}(i)=\begin{cases}1, & i=a_j^{(\zeta)}, j=0,1,\cdots,2KN_{\mathrm{f}}-1;\\ 0, & \text{others}\end{cases} \tag{12}$$

where $a_j^{(\zeta)}$ is the THSI of the ζ-th SIT.

5.3 Pulse Position Detection of the PL Signal

After obtaining the mapped binary code sequences of auto-correlation peak intervals and total N stored SITs, the pulse positions of the transmitted PL signal can be easily detected by the circular correlation operation. The detailed detection process is given as

$$p^{(\hat{\zeta})}=\arg\underset{i,\zeta}{\left(\max\max_{\substack{i=0,1,\cdots,L-1;\\ \zeta=1,2,\cdots,N}}\left(\bar{\mathbf{H}}(i)\otimes\tilde{\mathbf{B}}^{(\zeta)}(i)\right)\right)} \tag{13}$$

where $\hat{\zeta}$ is the estimated SIT group ID used by the PL signal; "$\otimes$" denotes the circular correlation; $\bar{\mathbf{H}}(i)$ and $\tilde{\mathbf{B}}^{(\zeta)}(i)$ denote the code sequences of $\bar{\mathbf{H}}$ and $\tilde{\mathbf{B}}^{(\zeta)}$ after i circular shift, respectively. Here $\bar{\mathbf{H}}$ and $\tilde{\mathbf{B}}^{(\zeta)}$ are respectively the interpolated sequences of $\mathbf{H}$ and $\mathbf{B}^{(\zeta)}$ [9].

6. Performance Simulations of the Formed SITs

To verify the SIT performance of the proposed method, simulations on THSI distributions, correlation and power spectral density (PSD) properties of the generated SITs, and SIT detection of the PL signal in receiving end are carried out with software MATLAB® 2016b (SIT generation codes of the proposed method have been uploaded to website given below[1]). For comparisons, the simulation results of SITs given by the Locata scheme [3] and random permutation (RP) method [2], [9] under the same conditions are also presented.

In Sec. 6.1 to 6.3, the main simulation parameters are set up as: $d=0.1$, $N_{\mathrm{f}}=10$, $K=10$, PRN code period $T_{\mathrm{c}}=1$ ms in which $L_{\mathrm{c}}=1023$ chips are included, PL pulse duration $T_{\mathrm{p}}=T_{\mathrm{c}}d=0.1$ ms, data bit periods of GNSS-like signal and PL signal are 20 ms and 200 ms, respectively. While in Sec. 6.4, referring to [9] the main simulation parameters are set up as:

- Sampling frequency of the received PL signal $f_{\mathrm{s}}=12$ MHz, the intermediate frequency $f_{\mathrm{IF}}=4.309$ MHz, and the Doppler frequency $f_{\mathrm{Dop}}=800$ Hz.
- The period of one TH frame $T_{\mathrm{c}}=1$ ms, thus for the pulsing scheme with duty cycle d, the pulse duration $T_{\mathrm{p}}=d$ ms. Meanwhile, during the SIT detection of the received PL signal, total 12 different SITs are generated with the proposed method and stored in the receiver, and the number of THSIs in each generated SIT is $2N_{\mathrm{f}}^2$.
- GPS C/A code is chosen as the PRN code of the PL signal, and its chip rate is set to $1.028/d$ Mchips/s for the given d. The initial phase of PRN code is set to $\tau_{\mathrm{prn}}=220$ chips. Additionally, due to the period of one PL data bit often equals that of one TH pulse pattern and only the SIT of one TH pulse pattern is mainly discussed in the paper, the PL data bit is set to 1 for simplicity in simulations.
- The 7-th SIT of total 12 generated SITs is chosen to form the transmitted PL signal, and the initial phase of the received PL signal is set to 8 time slots.

Other special parameters will be given in the detailed simulations.

6.1 Simulations on THSI Distribution of Different SITs

Just as what has been explained in Sec. 2, the THSI in each row of the base matrix randomly takes the value in the set $\{0,1,\cdots,N_{\mathrm{f}}-1\}$ once and only once, thus it is difficult to obtain the THSI distribution characteristic directly. As an alternative, the THSI intervals of different SITs are simulated, and the results of four random selected SITs are given in Figs. 4 and 5.

From Figs. 4 and 5 it can be got that: 1) although the average THSI interval of the proposed method is almost same as that of the Locata scheme, the former is more variable in standard error than the later, and this will bring benefit to the detection and track of the transmitted PL signal [10]; 2) for the proposed method the repetition times of THSI interval equals 10 are less than those for the Locata scheme, and this can reduce the chance of generating the false spectral lines during tracking the PL signal [2]. Of course, the Locata scheme also has an advantage in that the repetition times of THSI interval which equals 1 are 0, and this can avoid the detection ambiguity of two adjacent binary-mapped THSIs.

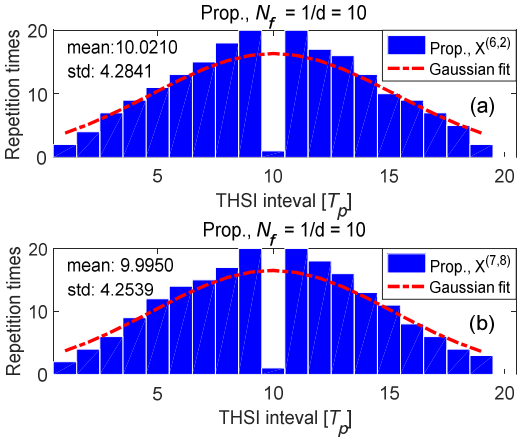

Fig. 4. Histograms of different SITs given by the proposed method.

[1]https://ww2.mathworks.cn/matlabcentral/fileexchange/123280-sitsgenpl

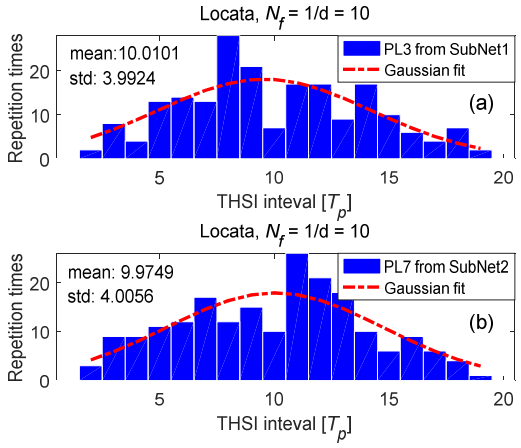

Fig. 5. Histograms of different SITs given by the Locata scheme.

6.2 Simulations on Correlation Properties of the Formed SITs

The correlation property of the formed SIT directly affects the detection performance of the generated PL signal. To verify the correlation performance of the proposed method, simulations on ACF and CCF properties of different SITs given by the proposed method, Locata scheme [3], [6], and RP method [2], [9] are carried out, and the results are shown in Figs. 6 to 8, in which both RTCM scheme [11] and Locata scheme can be regarded as RP methods considering their irregular THSI distribution in SITs, and the main difference between the two schemes is that the former only offers one SIT for use, while the latter offers multiple SITs for use and these SITs may have undergone optimal selection. In addition, for the better validation, the ACF-related parameter comparisons of the proposed method and the Locata scheme corresponding to Figs. 6 and 7 are also offered in Tab. 2, in which the PRN code ranging error is derived by combining average PRN chips which are not affected by THSI hits in one PRN code period with Eq. (27) of [4].

From Figs. 6 to 8 and Tab. 2, it is easily found that the ACF performance of the proposed method is better than that of RP methods including the Locata scheme and RTCM scheme, and the CCF performance of the proposed method is comparable to that of RP methods. More concretely, by comparison it easily seen that the maximum ACF subpeak of the proposed method given in Fig. 6 is lower than those of RP methods given in Fig. 8. While for the Locata scheme given in Fig. 7, though its ACF performance seems to be comparable to that of the proposed method, the results given in Tab. 2 show that the average PRN code ranging error of the proposed method is about 0.8 m and that of the Locata scheme is about 0.95 m, which means the proposed method outperforms the Locata scheme about 0.15 m, or improves about 16%. Here the ACF subpeak upper bound and CCF peak upper bound can be calculated as 0.19 (−14.42 dB) and 0.28 (−11.06 dB) by Theorem 3 and Corollary 1, respectively. To sum up, if both ACF and CCF performance is taken into account, the proposed method is relatively better than the RP methods including the Locata scheme and RTCM scheme.

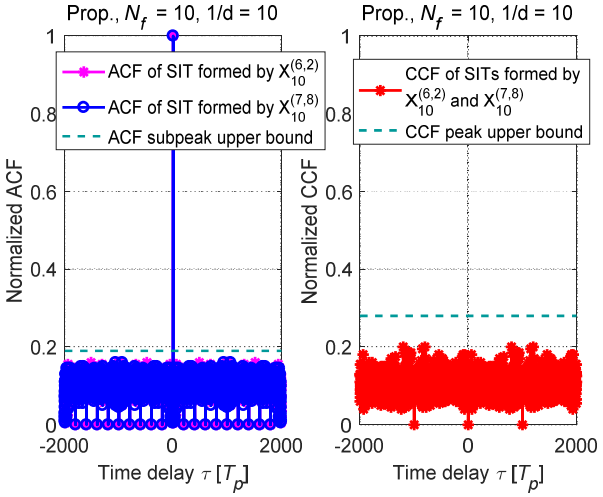

Fig. 6. ACF and CCF of different SITs given by the proposed method.

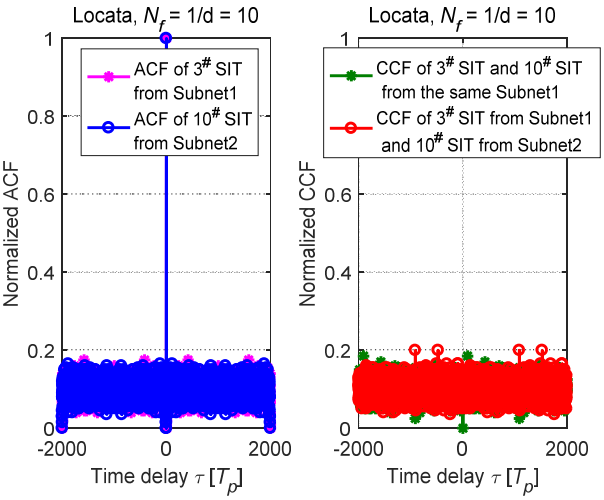

Fig. 7. ACF and CCF of different SITs given by the Locata scheme, in which the SIT is also called the device transmit sequence (DTS) in Locata ICD [3].

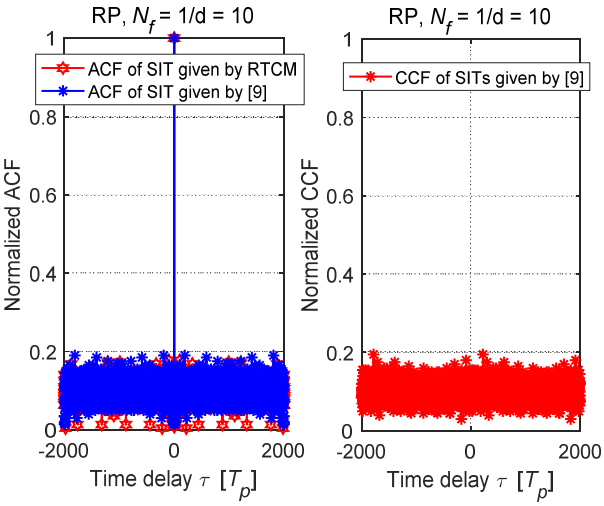

Fig. 8. ACF and CCF of different SITs given by the RTCM scheme and normal RP method [9].

Parameters	Proposed (Fig. 6)		Locata (Fig. 7)	
	$X_{10}^{(6,2)}$	$X_{10}^{(7,8)}$	3# SIT(Subnet1)	10# SIT(Subnet2)
Avg. unaffeced PRN chips in L_c	1015	1015	1011	1012
PRN code ranging error [m]	0.808	0.808	0.987	0.946

Tab. 2. ACF-related parameter comparisons of different SITs given by the proposed method and the Locata scheme.

Parameters	Proposed (Fig. 9)		Locata (Fig. 10)	
	$X_{10}^{(6,2)}$	$X_{10}^{(7,8)}$	3# SIT(Subnet1)	10# SIT(Subnet2)
Max subpeak [dB]	–15.49	–16.23	–15.12	–14.93
Avg. subpeak attenuation [dB]	34.25	34.28	26.77	26.65

Tab. 3. PSD-related parameter comparisons of different SITs given by the proposed method and the Locata scheme.

6.3 Simulations on PSD of the Formed SITs

To further verify the performance of the formed SITs, simulations on PSD of different SITs given by the proposed method and RP methods including the Locata scheme and RTCM scheme are also carried out, and the results are shown in Figs. 9 to 11. In addition, considering the SIT performance of the Locata scheme is better than that of the normal RP methods because the SITs given by the Locata scheme may have undergone optimal selection, the PSD-related parameter comparisons corresponding to Fig. 9 of the proposed method and Fig. 10 of the Locata scheme are offered in Tab. 3.

From Figs. 9 to 11 it is easily found that the PSD performance of the proposed method is also better than that of RP methods including the Locata scheme and RTCM scheme. More specifically, it can be seen that the PSD subpeak attenuation of the proposed method given in Fig. 9 is higher than that of the Locata scheme given in Fig. 10 and RP methods including the RTCM scheme given in Fig. 11, and the parameter comparisons on average subpeak attenuation of the proposed method and the Locata scheme given in Tab. 3 can also embody this point. For example, the parameter of average subpeak attenuation of SITs give by the proposed method is about 34 dB, while for the SITs given by the Locata scheme this value is about 26 dB, which means the proposed method outperforms the Locata schemes about 8 dB, or improves about 31%. This PSD performance of the proposed method lays a good foundation for the detection and track of the transmitted PL signal in the receiver.

6.4 Simulations on SIT Detection of the Received PL Signal

To obtain SIT detection performance of the received PL signal, based on the explanations and detection steps given in Sec. 5, the detection probability and detection error of TH pulse initial phase of different SITs generated by the proposed method and RP methods are simulated, and the results are shown in Figs. 12 and 13. Besides, to give more insight into SIT detection performance, the tracking results of the PL signal generated with different SITs are also simulated, and the results are shown in Figs. 14 and 15, in which the results given in Fig. 14 are used to examine the interference of PL signal on the tracking of GNSS signal under different conditions. Note that in Figs. 12 to 15, the SITs generated with normal RP method instead of the Locata scheme or RTCM scheme have been used for comparisons, and this is because the Locata scheme or RTCM scheme only offers the SITs for $d = 1/10$.

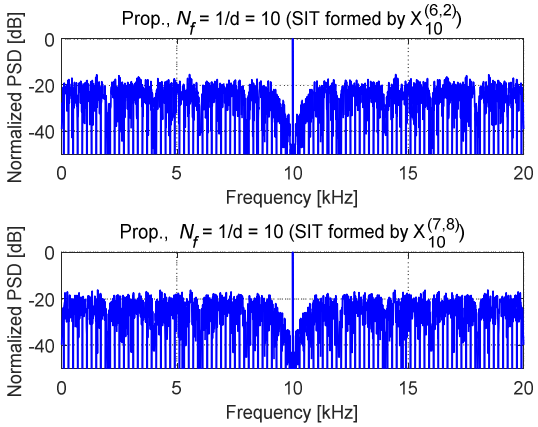

Fig. 9. PSD of different SITs given by the proposed method.

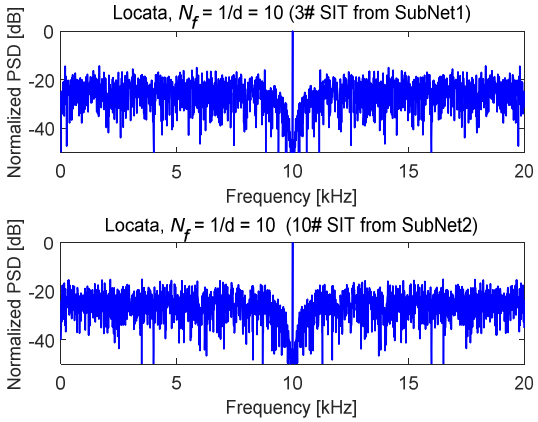

Fig. 10. PSD of different SITs given by the Locata scheme.

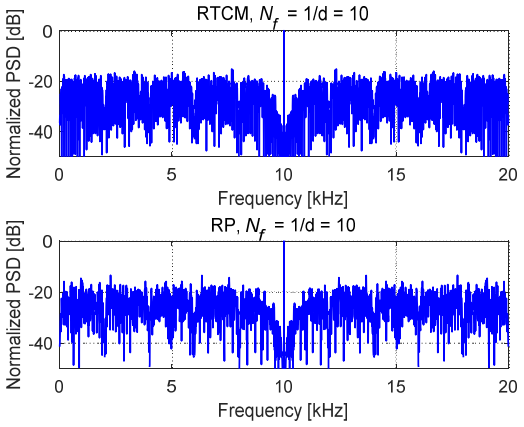

Fig. 11. PSD of different SITs given by the normal RP methods.

From Fig. 12 it can be seen that under the same d and signal to noise ratio (SNR), TH initial phase detection probability of the SIT given by the proposed method outperforms that of the SIT given by the RP method. For example, under $d = 1/22$ and SNR $= -10$ dB, the detection probability of the proposed method is about 0.9, and this result will fall to 0.2 for the RP method. On the other hand, as for TH pulse initial detection error given in Fig. 13, the same conclusion that the proposed method outperforms the RP method can be drawn. For example, under $d = 1/10$ and SNR $= -11$ dB, TH pulse initial phase detection error of the proposed method is about 0.5 µs, but for the RP method this result is larger than 3 µs. The reason that SIT detection performance of the proposed method is better than that of the RP method can be explained by the relatively better ACF and PSD performance offered by the proposed method.

Besides in detection probability and detection error, the proposed method also outperforms the RP method in delay-locked loop (DLL) tracking error, as can be seen from Figs. 14 and 15. In Fig. 14, it is shown that under the same d and SNR of PL signal, for the proposed method GNSS tracking result is better than that for the RP method. For example, under $d = 1/10$ and PL SNR $= 10$ dB, when GNSS SNR $= -10$ dB, the DLL tracking root mean square error (RMSE) of GNSS signal equals 2.4 m for the proposed method, but for the RP method this result becomes 2.6 m. On the other hand, when the tracked PL signal is overlapped with GNSS signal, the proposed method can also give the relatively better tracking result compared with the RP method, as can be easily seen from Fig. 15. The relatively better tracking results of the proposed method given in Figs. 14 and 15 can be explained by that the proposed method has relatively lower THSI hits or more unaffected PRN chips compared with the RP method, as shown in Tab. 2.

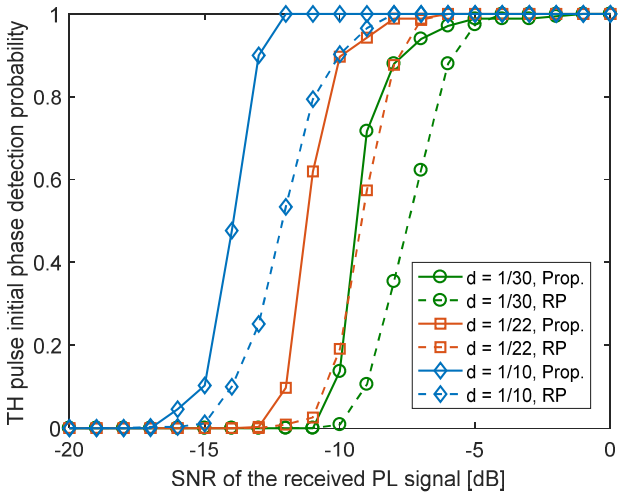

Fig. 12. TH pulse initial phase detection probability of different SITs generated by the proposed method and RP method.

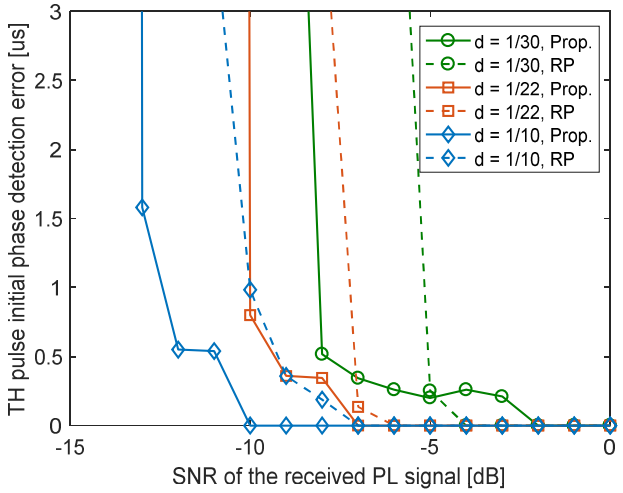

Fig. 13. TH pulse initial phase detection error of different SITs generated by the proposed method and RP method.

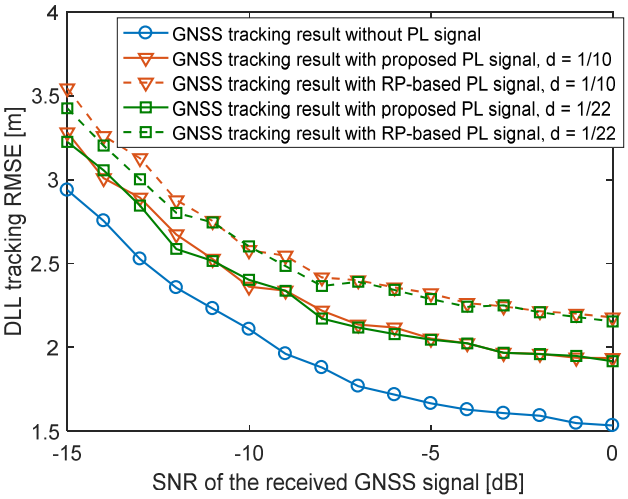

Fig. 14. GNSS signal tracking results when overlapped with PL signal, in whhich the PL signal is generated by the proposed method or by RP method, and the SNR of the PL signal equals 10 dB.

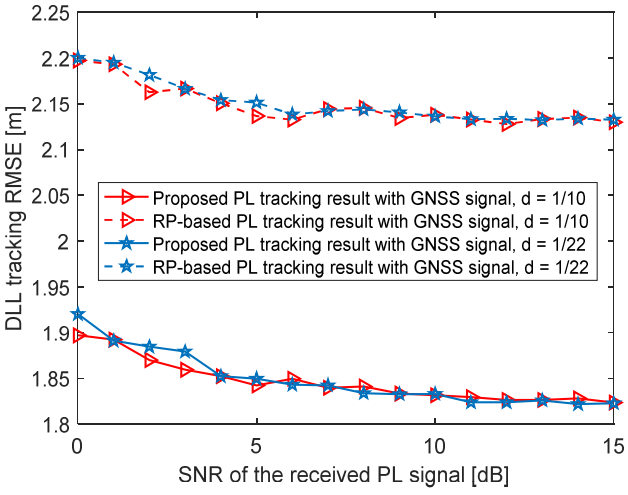

Fig. 15. PL signal tracking results of the proposed method and RP method when overlapped with GNSS signal, in which the SNR of GNSS signal equals –10 dB.

7. Conclusions

A new method using the constructed congruence codes to generate the THSI base matrices and then using these generated THSI base matrices to form the SITs of different TH pulsed PLs is proposed. The simulations show that compared with other similar SIT generation schemes, the proposed method can gain better performance in THSI distribution characteristic, correlation property, SIT detection and so on. On the other hand, due to the discontinuous property of the generated TH pulsed PL signal, the acquisition and tracking of this PL signal is often more complicated than the same processing of continuous GNSS signal. For example, the optimal carrier tracking loop of this PL signal will be Kalman filter-based variable update rate loop (KF-VURL) [17] instead of the normal phase-locked loop (PLL). To these problems, more work will be carried out combining with the proposed PL signal in the future.

Acknowledgments

This work was supported by the Open Research Fund of State Key Laboratory of Satellite Navigation System & Equipment Technology under grant CEPNT-2017KF-06. The authors also would like to acknowledge the anonymous reviewers for their constructive comments.

References

[1] LIU, X., YAO, Z., LU, M. Robust time-hopping pseudolite signal acquisition method based on dynamic Bayesian network. *GPS Solutions*, 2021, vol. 25, no. 2, p. 1–14. DOI: 10.1007/s10291-020-01066-y

[2] BORIO, D., O'DRISCOLL, C. Design of a general pseudolite pulsing scheme. *IEEE Transactions on Aerospace & Electronics System*, 2014, vol. 50, no. 1, p. 2–16. DOI: 10.1109/TAES.2013.110277

[3] LOCATA CORP. *Locata Signal Interface Control Document, Locata-ICD-100E*, Griffith(Australia): Locata corporation, 2014.

[4] O'DRISCOLL, C., BORIO, D., FORTUNY-GUASCH, J. Investigation of pulsing schemes for pseudolite applications. In *Proceedings of the 24th International Technology Meeting of ION*. Portland (USA), 2011, p. 3480–3492.

[5] HU, Y., SONG, M., DANG X., et al. Interference mitigation for the GPS receiver utilizing the cyclic spectral analysis and RR-MSWF algorithm. *Radioengineering*, 2017, vol. 26, no. 3, p. 798–807. DOI: 10.13164/re.2017.0798

[6] CHEONG, J. W. *Signal Processing and Collective Detection for Locata Positioning System. Ph.D. Thesis*. University of New South Wales, Australia, 2012. DOI: 10.26190/unsworks/15552

[7] YUN, S., YAO, Z., WANG, T., et al. High accuracy and fast acquisition algorithm for pseudolites-based indoor positioning systems. In *The 4th International Conference on Ubiquitous Positioning Indoor Navigation and Location Based Services*. Shanghai (China), 2016, p. 51–60. DOI: 10.1109/UPINLBS.2016.7809950

[8] TAO, L., SUN, J., LI, G., et al. An improved navigation pseudolite signal structure based on the Kasami sequences and the pulsing scheme. *Chinese Jouranl of Electronics*, 2022, vol. 31, no. 2, p. 220–226. DOI: 10.1049/cje.2020.00.403

[9] HU, Y., YU, B., SONG, M., et al. Pulse position detection of the pseudorandom time-hopping pseudolite for the participative GNSS receivers. *IEEE Access*, 2020, vol. 8, p. 216151–216161. DOI: 10.1109/ACCESS.2020.3040960

[10] ABT, T. L., SOUALLE, F., MARTIN, S. Optimal pulsing schemes for Galileo pseudolite signals. In *Proceedings of the 18th International Technical Meeting of the Satellite Division of ION*. Long Beach (USA), 2007, p. 926–934.

[11] STANSELL, T. A. RTCM SC-104 recommended pseudolite signal specification. *Navigation, Journal of the Institute of Navigation*, 1986, vol. 33, no. 1, p. 42–59. DOI: 10.1002/j.2161-4296.1986.tb00923.x

[12] MARIC, S., TITLEBAUM, E. L. A class of frequency hop codes with nearly ideal characteristics for use in multiple-access spread-spectrum communications and radar and sonar systems. *IEEE Transactions on Communications*, 1992, vol. 40, no. 9, p. 1442–1447. DOI: 10.1109/26.163565

[13] KOSTIC, Z., TITLEBAUM, E. L. The design and performance analysis for several new classes of codes for optical synchronous CDMA and for arbitrary-medium time-hopping synchronous CDMA communication systems. *IEEE Transactions on Communincations*, 1994, vol. 42, no. 8, p. 2608–2617. DOI: 10.1109/26.310621

[14] WEI, Z., SHALABY, H. M. H., GHAFOURI-SHIRAZ, H. Modified quadratic congruence codes for fiber Bragg-grating-based spectral-amplitude-coding optical CDMA systems. *Journal of Lightwave Technology*, 2001, vol. 19, no. 9, p. 1274–1281. DOI: 10.1109/50.948274

[15] YANG, G. C., KWONG, W. C. *Prime Codes with Applications to CDMA Optical and Wireless networks* (p. 44–48). Boston (USA): Artech House, 2002. ISBN: 9781580530736

[16] BORE, K., AKOS, D. M., BERTELSEN, N., et al. *A Software-Defined GPS and Galileo Receiver: A Single-Frequency Approach* (p. 75–86). Boston (USA): Birkhauser, 2006. ISBN: 9780817643904

[17] YUN, S., YAO, Z., LU, M. Variable update rate carrier tracking loop for time-hopping DSSS signals. *IET Radar, Sonar and Navigation*, 2019, vol. 13, no. 6, p. 961–968. DOI: 10.1049/iet-rsn.2018.5566

About the Authors . . .

Yi HU was born in Lu'an, China, in 1974. He is currently an Associate Professor in Department of Mechanical & Electrical Engineering of Chuzhou University. He received his Ph.D. degree from Nanjing University of Aeronautics & Astronautics (NUAA) in 2015. His research interests include satellite navigation signal processing and Sat-COM.

Baoguo YU was born in Inner Mongolia, China, in 1966. He is a Research Professor and Director in State Key Laboratory of Satellite Navigation System & Equipment Technology. His current research interests include satellite navigation signal processing techniques and Sat-COM.

Zhixin DENG was born in Shijiazhuang, China, in 1982. He is a Senior Engineer in State Key Laboratory of Satellite Navigation System & Equipment Technology. His current research interests include satellite navigation signal processing techniques and wireless communications.

Wenjuan YU was born in Heilongjiang, China, in 1990. She is a Lecturer in Department of Mechanical & Electrical Engineering of Chuzhou University. Her current research interests include signal and information processing techniques.